Vibrational and Electronic Absorption Spectroscopy of Dibenzo[*b,def*]chrysene and Its Ions

Haiyan Wang, Jan Szczepanski, So Hirata, and Martin Vala*

Department of Chemistry and Center for Chemical Physics, University of Florida, Gainesville, Florida 32611-7200

Received: May 26, 2005; In Final Form: September 7, 2005

The vibrational and electronic absorption spectra of dibenzo[*b,def*]chrysene (DBC) and its ions in argon matrixes have been recorded. Assignment of the observed infrared (IR) bands has been made by comparison with the density functional theory (DFT) computations of harmonic vibrational frequencies (with 6-31G(d,p) or 6-311+G(d,p) basis sets). Extensive time-dependent (TD) DFT calculations of vertical excitation energies have aided in the assignment of the experimental electronic absorption transitions. In general, the theoretical predictions are in good agreement with the observed ultraviolet and visible bands. By correlating IR and UV−visible band intensities (after UV photolysis), it has been shown that both DBC cations and anions are formed. The IR band intensity distributions of the DBC ions differ markedly from neutral DBC. A synthetic spectrum composed of neutral, cationic, and anionic DBC contributions compares reasonably well with the interstellar features of the "unidentified infrared" (UIR) bands from the reflection nebula NGC 7023. Finally, it is shown that the electronic absorption bands of the DBC ions lie in close proximity to several of the diffuse interstellar visible absorption bands (DIBs).

I. Introduction

Polycyclic aromatic hydrocarbons (PAHs) are stable compounds composed of six (or five)-membered carbon rings. Due to their adverse effects on human health, considerable effort has been devoted to studies of PAHs in the analytical, biological, and medical sciences. Techniques for monitoring PAHs in the environment have been developed, and mechanisms for their influence on the human body have been proposed.[1−4]

Recently, the spectra and structure of PAHs have undergone intense study because of their probable importance in the field of astrochemistry. This interest arose because of the suggestion by Leger and Puget, and Allamandola and co-workers, that PAHs might be responsible for the unidentified infrared (UIR) interstellar emission bands.[5,6] This idea has now been widely accepted, although the mechanism of PAH formation in space remains uncertain. Indeed, PAHs are regarded as among the most abundant free organic molecules in space. They have also been proposed, together with unsaturated carbon chains and rings, as the carriers of the diffuse interstellar visible absorption bands (DIBs). Neutral, dehydrogenated, and ionized PAH species, including their coordination compounds, may also be present in space.[6] However, to date, no individual PAH species has been positively identified in space except for the single ring species, benzene.[7] Although spectral data are available only for a limited number of PAHs, it is generally believed that the UIR (and DIB) bands can be attributed to the emission (or absorption) of hydrocarbon compounds containing between 20 and 100 (or more) carbon atoms.[5,8] Constraints due to bandwidths, anharmonicities, and isotopic shifts from laboratory data hinder further astrophysical identification.[7] Current understanding holds that the UIR bands originate from a mixture of PAHs (a PAH "soup"), which makes their individual identification and/or simulation problematic.[9]

Dibenzo[*b,def*]chrysene (DBC) has been studied previously using a number of techniques.[10−14] However, the vibrational and electronic spectra of neutral DBC and its ions, coupled with high-level theoretical calculations, have not yet been reported. In this paper, we report on the infrared and electronic spectra of neutral, cationic, and anionic DBC trapped in solid argon at 12 K. Spectral assignments are supported by density functional theory (DFT) calculations of vibrational harmonic frequencies and time-dependent electronic transition energies.

II. Experimental Procedures

Infrared and electronic absorption spectra of neutral DBC and its radical ions were recorded using the same experimental apparatus as described in our previous PAH studies.[15] In brief, solid DBC powder (Sigma-Aldrich, Inc.) was vaporized from a quartz oven heated to around 300 °C. DBC vapor was trapped with argon (99.995% purity, Matheson) and deposited on a BaF_2 window cooled to 12 K by a closed-cycle helium cryostat. After deposition for 2−4 h, the infrared absorption spectrum (4000−700 cm^{-1}) was recorded using a MIDAC M2000 FT-IR spectrometer with 1 cm^{-1} resolution. Thereafter, the electronic absorption spectrum (900−200 nm) of the same matrix was collected with an IBM 9420 UV−visible spectrophotometer at 0.28-nm resolution.

Using a homemade electron gun located ca. 3 cm from the BaF_2 sample window, DBC ions were generated and deposited with the neutral species in an argon matrix. The electrons were accelerated toward the deposition region by a +90 V O-ring electrode located 5 mm in front of the cryostat window. The electron beam current (ca. 50−70 μA) was monitored using a microammeter connected in series with the ring electrode. Cation formation proceeded via Penning ionization, giving Ar* metastable species, and via charge transfer (CT), giving Ar^+−DBC CT complexes. The high electron affinity of DBC makes anion formation also possible. To obtain the highest possible ratio of cations to neutral species, the electron scavenger carbon

* To whom correspondence should be addressed. E-mail: mvala@chem.ufl.edu.

10.1021/jp0527960 CCC: $30.25
Published on Web 10/12/2005

tetrachloride, CCl_4 (Kodak, Spectrograde), was seeded into the argon gas (99.7% Ar, 0.3% CCl_4). A lengthy deposition (typically 4 h) was required to achieve a high concentration ratio of ions to neutrals. Finally, the matrix was rescanned after either matrix annealing (to 35 K) or photolysis (100 W medium-pressure Hg lamp). A correlation between the resulting infrared (IR) and UV−visible spectral band intensities was used to confirm the identification of cations and anions.

III. Computational Methods

Geometries, energies, and harmonic vibrational frequencies were calculated with the Gaussian 98 suite of programs using the density functional theory (DFT).[16] Previous work showed that the 6-31G(d,p) basis set is large enough to account for most features of the PAHs and their ions. However, the larger 6-311+G(d,p) basis set generally yields more accurate frequencies and intensities. Therefore, either the 6-31G(d,p) or the 6-311+G(d,p) basis set was applied to neutral DBC using the B3LYP theory (Becke's three-parameter hybrid functional combined with Lee−Yang−Parr correlation functional), whereas only the 6-31G(d,p) basis set was employed for the DBC ions.

Vertical excitation energies and oscillator strengths of neutral DBC and its ions were computed by the time-dependent (TD) DFT method using the B3LYP functional with the 6-31G(d,p) basis set. To monitor the accuracy of the vertical excitation energies using the Gaussian 98 platform, all excited-state calculations were also carried out with massively parallel DFT and TDDFT implementations of the NWCHEM quantum chemistry software suite,[17] now widely used in modeling the excited states of PAHs.[18] Vertical excitation energies and oscillator strengths of the neutral, cationic, and anionic species of DBC were computed by TDDFT using the Becke−Lee−Yang−Parr (BLYP) and asymptotically corrected Becke3−Lee−Yang−Parr [B3LYP(AC)] functionals in conjunction with the 6-31G(d,p) basis set. Geometries were optimized in the ground states using the B3LYP functional and the 6-31G(d,p) basis set (for the neutral and cation) and the 6-31++G(d,p) basis set (for the anion). Generally, TDDFT is capable of reproducing the excitation energies of low-lying valence excited states of closed- and open-shell PAHs within 0.3 eV and the corresponding oscillator strengths only qualitatively.[18] The asymptotic correction algorithm[19] employed in this work automatically adjusts the depth of the exchange-correlation potentials in the valence region before splicing a $-1/r$ asymptotic tail to it, relying on a phenomenological linear relationship between the ionization potential and highest occupied orbital energies of B3LYP DFT calculations.[20] Excited-state roots were sought in each calculation using the Davidson trial vector algorithm. Twenty roots for neutral DBC and 10 roots for its cation and anion are given in Tables 2, 5, and 6, respectively.

IV. Results and Discussion

Figure 1 presents the optimized geometry found for neutral DBC (C_{2h} symmetry) calculated at the B3LYP/6-31G(d,p) level. DBC ions still retain C_{2h} symmetry, with similar bond lengths and angles. The C−C (C−H) bond length is ∼1.4 (1.1) Å, and the C−C−C and C−C−H bond angles are close to 120°, with deviations smaller than 5°. These parameters are typical of six-membered PAH rings. The values shown in the figure are C−H bond energies (eV) for DBC neutral and for its cation (in brackets), all calculated at the B3LYP/6-31G(d,p) level. The smallest C−H bond energy in neutral DBC is ∼4.7 eV, which is only 0.1 eV lower than for the other C−H bonds. The C−H bond in the DBC cation is stronger, with energies ranging between 5.47 and 5.92 eV. The dehydrogenation energies of neutral or cationic DBC are typical for the H-atom loss from sp^2 carbons but much higher than from sp^3 carbons.[21] Thus, removal of hydrogens from neutral or cationic DBC is expected to be more difficult than from 2,3-benzofluorene or fluorene, where hydrogen atoms were relatively easily removed from the sp^3 carbon.[21]

Dibenzo[b,def]chrysene (DBC), $C_{24}H_{14}$

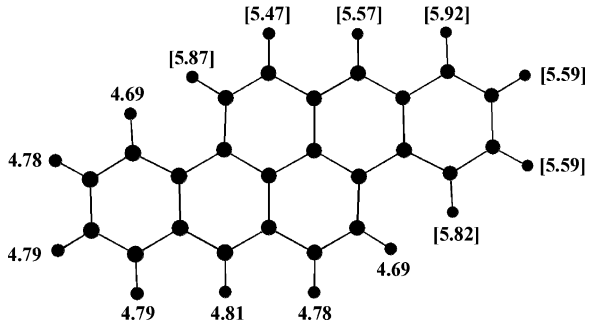

Figure 1. Equilibrium geometry of dibenzo[*b*,*def*]chrysene (DBC) calculated at the B3LYP/6-31G(d,p) level. Dehydrogenation zero-point corrected energies (in eV, B3LYP/6-31G(d,p)) for the neutral DBC and its cation (in brackets).

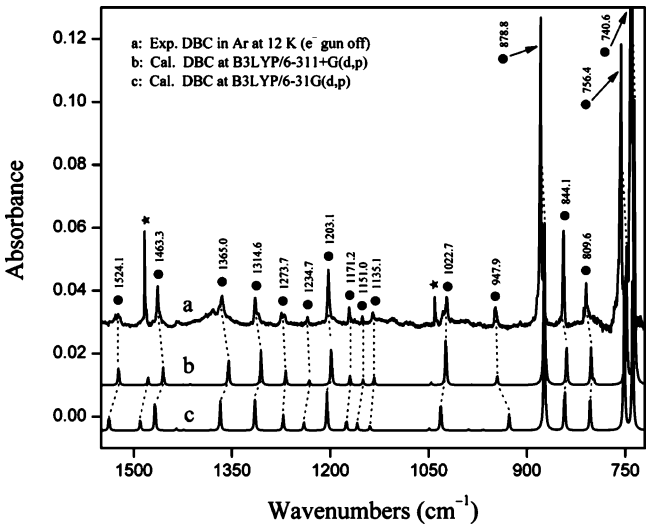

Figure 2. Experimental and calculated IR absorption spectra for neutral DBC. (a) IR absorption spectrum of DBC trapped in solid argon at 12 K. (b) IR spectrum calculated at the B3LYP/6-311+G(d,p) level (scaled by 0.978). (c) IR spectrum calculated at the B3LYP/6-31G(d,p) level (scaled by 0.978).

A. Neutral DBC. *1. Infrared Absorption Spectra.* The experimental vibrational spectrum of neutral DBC isolated in an Ar matrix at 12 K is displayed in Figure 2. Calculated spectra are also included for comparison. Experimental and calculated band frequencies, relative intensities, and mode descriptions are listed in Table 1. To account for vibrational anharmonicity and basis set deficiencies, the B3LYP frequencies were scaled by a factor of 0.978.[22] Only those bands with relative intensities larger than 2% are tabulated.

All observed bands could be assigned to predicted frequencies except for two, marked with ★ (in Figure 2). Satisfactory agreement was also obtained between the predicted frequencies and a few bands below 700 cm^{-1} observed for DBC in a KBr matrix at room temperature (cf. Table 1). In the 700−1400 cm^{-1} region, band positions predicted via B3LYP/6-311+G(d,p) calculations fit slightly better, with less than a 10 cm^{-1} discrepancy. Although the predicted frequencies (using B3LYP/

TABLE 1: Comparison of the Calculated and Experimental (Ar matrix, 12 K) Infrared Absorption Bands (in cm^{-1}) of Neutral Dibenzo[*b*,*def*]chrysene in the ^1A_g Electronic Ground State

symmetry	mode description[b]	ν_{cal}[a,c]	ν_{cal}[a,d]	ν_{exp}[a]
b_u	α(C−C−C)	162.3 (0.02)	162.1 (0.02)	
a_u	τ(C−C−C)	164.1 (0.05)	161.0 (0.08)	
b_u	α(C−C−C)	471.4 (0.07)	470.1 (0.08)	
a_u	τ(C−C−C)	475.6 (0.13)	470.5 (0.23)	473.7 (0.27)[e]
b_u	α(C−C−C)	512.5 (0.13)	512.4 (0.12)	514.6 (0.10)[e]
b_u	α(C−C−C)	635.4 (0.31)	635.2 (0.25)	634.8 (0.42)[e]
a_u	ϵ(C−C−H) + τ(C−C−C)	675.3 (0.14)	667.6 (0.26)	679.1 (0.60)[e]
a_u	ϵ(C−C−H)	738.6 (0.97)	736.0 (1.57)	740.6 (1.31)
a_u	ϵ(C−C−H)	751.5 (0.86)	748.1 (0.75)	756.4 (0.87)
b_u	α(C−C−C)	752.4 (0.06)	752.1 (0.04)	
b_u	α(C−C−C)	803.5 (0.20)	802.0 (0.21)	809.6 (0.12)
a_u	ϵ(C−C−H)	842.4 (0.25)	839.4 (0.24)	844.1 (0.32)
a_u	ϵ(C−C−H)	873.4 (1.00)	873.4 (1.00)	878.8 (1.00)
b_u	α(C−C−C)	873.4 (0.07)	873.5 (0.06)	
a_u	ϵ(C−C−H)	927.1 (0.09)	945.4 (0.06)	947.9 (0.06)
b_u	*R*(C−C) + α(C−C−C)	1031.5 (0.17)	1023.7 (0.27)	1022.7 (0.09)
b_u	β(C−C−H)	1139.6 (0.03)	1133.3 (0.05)	1135.1 (0.03)
b_u	β(C−C−H)	1158.8 (0.04)	1150.0 (0.03)	1151.0 (0.03)
b_u	β(C−C−H)	1175.5 (0.06)	1170.0 (0.05)	1171.2 (0.05)
b_u	β(C−C−H)	1205.1 (0.23)	1198.6 (0.23)	1203.1 (0.17)
b_u	β(C−C−H) + *R*(C−C)	1240.3 (0.05)	1232.2 (0.03)	1234.7 (0.02)
b_u	β(C−C−H)	1272.0 (0.09)	1268.1 (0.08)	1273.7 (0.04)
b_u	β(C−C−H) + *R*(C−C)	1315.2 (0.18)	1305.9 (0.19)	1314.6 (0.09)
b_u	*R*(C−C) + β(C−C−H)	1368.0 (0.17)	1355.4 (0.15)	1365.0 (0.07)
b_u	β(C−C−H) + *R*(C−C)	1467.6 (0.17)	1455.1 (0.10)	1463.3 (0.13)
b_u	β(C−C−H) + *R*(C−C)	1490.6 (0.07)	1478.3 (0.04)	
b_u	*R*(C−C) + β(C−C−H)	1538.4 (0.08)	1523.7 (0.10)	1524.1 (0.04)
b_u	*R*(C−C) + β(C−C−H)	1601.8 (0.06)	1587.0 (0.06)	
b_u	*R*(C−C) + β(C−C−H)	1611.6 (0.05)	1595.0 (0.03)	
b_u	*R*(C−C) + β(C−C−H)	1639.7 (0.25)	1622.4 (0.16)	*f*
b_u	*r*(C−H)	3103.7 (0.08)	3088.3 (0.06)	2861.5 (0.09)[g]
b_u	*r*(C−H)	3108.4 (0.12)	3092.5 (0.07)	
b_u	*r*(C−H)	3112.0 (0.44)	3096.1 (0.33)	
b_u	*r*(C−H)	3118.3 (0.79)	3101.9 (0.63)	
b_u	*r*(C−H)	3132.8 (1.54)	3116.2 (1.06)	2933.3 (1.08)[g]
b_u	*r*(C−H)	3143.4 (0.34)	3127.9 (0.18)	
b_u	*r*(C−H)	3158.1 (1.25)	3143.5 (0.77)	2966.1 (0.55)[g]

[a] Relative IR intensities for predicted and experimental frequencies are given in parentheses. [b] Notation used: *R* and *r* are stretching modes, α and β are in-plane bending modes, and τ and ϵ are out-of-plane vibrations. [c] Calculations were carried out at B3LYP/6-31G(d,p) level, and all frequencies were scaled by a factor of 0.978. Only bands with relative intensities equal to or higher than 0.02 are listed. The integral intensity predicted for the 873.4 cm^{-1} band is 49.55 km/mol. [d] Calculations were at the B3LYP/6-311+G(d,p) level, and all frequencies were scaled by a factor of 0.978. Only bands with relative intensities equal to or higher than 0.02 are listed. The integral intensity predicted for the 873.4 cm^{-1} band is 57.72 km/mol. [e] Recorded from the solid mixture of DBC and KBr at room temperature. [f] Overlapped with water-bending vibration bands. [g] Very broad absorption bands in this region; bandwidth was considered for the estimate of their relative intensities.

6-31G(d,p)) exhibit slightly larger differences, they are reliable and accurate enough to make band assignments. Although all bands in this region were observed in both Ar matrixes and KBr pellets, much sharper bands were recorded in the matrix isolation experiments. In the C−H stretching region (3000−3100 cm^{-1}), however, a discrepancy of ∼120−180 cm^{-1} is invariably seen, indicating strong anharmonicities for these modes; thus, a different scaling factor (∼0.91−0.92) should be considered for this region. Because of the broadness of the band profiles in this region, these assignments should still be considered tentative, even though these bands were also seen in the room-temperature spectrum of DBC in KBr. As Table 1 shows, the C−C−H out-of-plane bending vibrations are stronger than other vibrational modes. The strongest experimental absorption is observed at 740.6 cm^{-1}. Theoretically, the C−C−H out-of-plane bending vibration at 873.4 cm^{-1} is very close to the C−C−H in-plane bending vibration at 873.5 cm^{-1}. However, the intensity of the former is much stronger than the latter. On the other hand, experimentally these two bands merge into one. The two bands at 1483.2 and 1040.7 cm^{-1} (★ in Figure 2) probably arise from thermal decomposition products because neither appears in the room-temperature spectrum of DBC in KBr nor do they track the DBC absorption band intensity in different experiments. Furthermore, their intensities, relative to the DBC bands, depend on the sample temperature.

The IR spectrum of neutral DBC was previously recorded using a linear dichroism (LD) technique in a thick polyethylene sheet.[12] Most bands observed in this work were reproduced in our matrix experiments except for two, at 769 and 976 cm^{-1}. Our theoretical calculations predict no absorption close to these positions, casting doubt on the origin of these peaks. There are, of course, small frequency differences between the LD and Ar matrix peaks. Some features could not be observed in the LD experiments because of substrate absorption, viz., the band at 1135.1 cm^{-1} and all higher bands (i.e., >1250 cm^{-1}).

2. Electronic Absorption Spectra. Neutral DBC has strong absorption bands in the UV−visible region (cf. Figure 3). The observed and theoretical vertical excitation energies and oscillator strengths of neutral DBC are compared in Table 2. The electronic transitions were assigned by comparing the observed absorption bands to the TDDFT-calculated vertical excitation energies and oscillator strengths (cf. Table 2 and Figure 3).

The observed energy for the $S_1 \leftarrow S_0$ transition is 2.83 eV (438.8 nm), which is close to the predicted value of 2.6−2.9 eV. Vibrational structure is observed on the first electronic absorption band (cf. the enlargement in Figure 3). The 433.7,

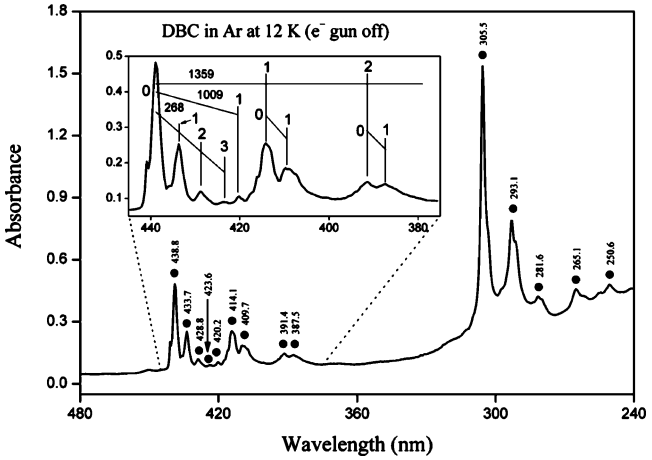

Figure 3. Electronic absorption spectrum of neutral DBC (Ar, 12 K) with band positions marked in nm. Insert spectrum shows the $S_1(^1B_u) \leftarrow S_0(^1A_g)$ transition. Band assignment is made on the basis of the 268, 1009, and 1359 cm^{-1} fundamental mode energies in S_1 state (see text).

420.2, and 414.1 nm bands are spaced 268, 1009, and 1359 cm^{-1} from the 438.8 nm (0−0) transition, respectively. Assuming no substantial conformational change in its S_1 state, the above intervals are well-described by ground-state Raman-active frequencies (scaled by 0.978). The 257 (56 Å^4/amu), 1032 (61 Å^4/amu), and 1365 cm^{-1} (522 Å^4/amu) bands match well with the observed intervals in the S_1 state and are thus considered part of the $S_1 \leftarrow S_0$ electronic transition. The absorption peaks at 428.8 and 423.6 nm are separated by $\sim 2 \times 268$ (531) and $\sim 3 \times 268$ (818) cm^{-1} from the 0−0 transition at 438.8 nm and are taken as the first and second overtones of the 268 cm^{-1} mode. Similarly, the 391.4 nm band is probably the first overtone of the 1359 cm^{-1} mode, because there is no corresponding Raman-active vibrational mode. The two remaining intervals associated with bands at 409.7 and 387.5 are assigned as combination modes: $1619 \approx 268 + 1359$ cm^{-1} and $3017 \approx 268 + 2 \times 1359$ cm^{-1}. The strongest absorption at 305.5 nm (4.06 eV) is assigned to the $S_7 \leftarrow S_0$ transition, and its two neighbor bands (293.1 and 281.6 nm), 1385 and 2778 ($\sim 2 \times 1385$) cm^{-1} from the 305.5 nm (0−0) band, can be ascribed to the predicted 1386 cm^{-1} (2490 Å^4/amu) Raman-active mode. The final two bands are close to the excitation energies of the $S_{11} \leftarrow S_0$ and $S_{13} \leftarrow S_0$ transitions. The transitions missing in the observed spectrum (e.g., $S_3 \leftarrow S_0$) are either due to symmetry restrictions or expected low oscillator strengths (cf. Table 2).

The calculated vertical excitation energies and oscillator strengths for the first 10 excited states are independent of the protocol used, Gaussian or NWChem (cf. Table 2). However, for the higher excited states, the results differ. Assignments for S_{11} and higher transitions should thus be regarded as tentative.

The two lowest-lying singlet excited states of neutral PAHs are, in order of increasing energy, usually ^1L_b and ^1L_a (in Platt nomenclature). The L_a state is primarily the HOMO to LUMO transition with a large oscillator strength, whereas the L_b state is a mixture of HOMO−1 to LUMO and HOMO to LUMO+1 promotions carrying a much smaller intensity. Parac and Grimme[23] found that the TDDFT methods often give incorrect ordering of these two states which, however, lie frequently within 0.3 eV of each other. It is therefore possible that the 2^1B_u state (so predicted by the TDDFT calculations), which is ^1L_b, in fact lies lower than the 1^1B_u state, which is ^1L_a. The assignment of the absorption band at 438.8 nm is based on the large intensity of the 1^1B_u state (^1L_a) and is unequivocal (although, if the ordering is incorrect, the transition should now be $S_2 \leftarrow S_0$). The weaker band due to the 2^1B_u state (^1L_b) may be overshadowed by this intense transition regardless of its precise position relative to that of the 1^1B_u state (^1L_a).

The oscillator strength (f) for an electronic transition can be calculated from the molar absorptivity (ϵ_{UV}) and the full width at half-maximum absorption ($\Delta\nu_{1/2}$) for each band:

$$f = 4.33 \times 10^{-9} \int \epsilon_{UV}(\nu)\mathrm{d}\nu \approx 4.33 \times 10^{-9} \sum \epsilon_{UV}(\nu)\Delta\nu_{1/2} \quad (1)$$

For the same sample/matrix, the molar absorptivity can be calculated from the relative IR and UV−visible band absorbance (A) using $\epsilon_{UV} = (A_{UV}/A_{IR})\epsilon_{IR}$. The IR molar absorptivity (ϵ_{IR}) can be obtained from the theoretical integral intensity, $I_{ab} = 2.303\epsilon_{IR}\Delta\nu_{1/2}$. For example, the well-isolated band at 878.8 cm^{-1} has a predicted (B3LYP/6-31G(d,p)) integral intensity of 50 km/mol. Because the observed bandwidth ($\Delta\nu_{1/2}$) is 2 cm^{-1}, the estimated ϵ_{IR} is 1086 M^{-1} cm^{-1}. The measured absorbance of the 878.8 cm^{-1} IR band is 0.0043, whereas the measured absorbance of the 438.8 nm band in the same matrix is 0.41 and the bandwidth is 105 cm^{-1}. Therefore, the expected molar absorptivity, ϵ_{UV}, for the 438.8 nm band is found to be 103.5×10^3 M^{-1} cm^{-1}. After summing the vibronic band contributions (cf. Figure 3), the oscillator strength (f) for the $S_1 \leftarrow S_0$ transition of neutral DBC is found to be 0.16. The f values for other electronic transitions of neutral and ionic DBC were determined similarly. The error in the f values comes mainly from the accuracy of the calculated integral IR intensities.

B. DBC Cation and Anion. *1. Infrared Absorption Spectra.* The infrared absorption spectra of neutral DBC and its cations and anions are given in Figure 4. Bands originating solely from neutral DBC are shown in the lower spectrum (c). The middle spectrum (b) shows the results after electron bombardment of the gas mixture (Ar/CCl_4). Bands corresponding to CCl_3, CCl_3^+, HAr_2^+, and the CCl_3·Cl complex are assigned on the basis of previous studies.[24−27] The new bands are mostly due to DBC cations. Because of its high electron affinity (2.0 eV),[28] CCl_4 acts as an electron scavenger with the result that the electrons from ionized DBC are trapped by CCl_4 and its byproducts, such as CCl_3 (2.6 eV),[29] CCl_2 (2.5 eV),[29] and Cl (3.6 eV).[30] All these byproducts have higher electron affinities than DBC (1.1 eV).[31] Almost no DBC anion bands are observed in this spectrum. Without CCl_4 in the gas mixture, absorption due to DBC anions (▽), cations (▼), and neutrals can be seen in the upper spectrum (a). The experimental band frequencies and theoretical values for DBC cations and anions, computed at the B3LYP/6-31G(d,p) level (and scaled by 0.978), are compared in Tables 3 and 4, respectively.

Like other PAH ions,[15,21,32] the intensities of the C−C stretching and C−C−H in-plane bending modes in the 1000−1600 cm^{-1} region are stronger than other vibrational modes. This is very different from neutral DBC, whose most intense bands lie in the C−H wagging region. No band attributable to the DBC cation is observed in the C−H stretching region, because its strongest predicted relative intensity is only 0.02. On the other hand, DBC anions have two C−H stretching modes in this region with computed relative intensities of 0.31 and 0.25. But, because of the band overlap in this region, peaks attributable solely to the anion could not be extracted from the experimental spectrum.

To show clearly the correlation between experimental and theoretical bands of the DBC ions, synthetic "experimental" spectra were constructed. A synthetic band, with half Gaussian

TABLE 2: Calculated and Observed Vertical Excitation Energies, ω, and Oscillator Strengths, f, for Neutral Dibenzo[*b*,*def*]chrysene[a]

		NWCHEM				Gaussian 98			
		B3LYP (AC)		BLYP		B3LYP		experiment	
state	transition[b]	ω/eV	f	ω/eV	f	ω/eV	f	ω/eV	f
^1B_u	$\pi_{-1} \rightarrow \pi_1^*$	2.90	0.3461	2.61	0.2358	2.69	0.2409	2.83 (438.8)[c] 2.77 (448.4)[d]	0.16[c]
^1B_u	$\pi_{-1} \rightarrow \pi_2^*$	3.26	0.0050	2.94	0.0032	3.25	0.0018		
^1A_g	$\pi_{-1} \rightarrow \pi_3^*$	3.62	inactive	3.02	inactive	3.61	inactive		
^1A_g	$\pi_{-1} \rightarrow \pi_4^*$	3.97	inactive	3.50	inactive	3.89	inactive		
^1A_g	$\pi_{-3} \rightarrow \pi_1^*$	4.15	inactive	3.69	inactive	4.06	inactive		
^1A_g	$\pi_{-4} \rightarrow \pi_1^*$	4.31	inactive	3.88	inactive	4.22	inactive		
^1B_u	$\pi_{-2} \rightarrow \pi_1^*$	4.35	1.4226	3.89	0.8626	4.12	1.1853	4.06 (305.5)[c] 3.96 (312.9)[d]	0.54[c]
^1A_g	$\pi_{-2} \rightarrow \pi_3^*$	4.50	inactive	4.03	inactive	4.49	inactive		
^1B_u	$\pi_{-5} \rightarrow \pi_1^*$	4.57	0.0071	3.92	0.0480	4.57	0.0011		
^1A_g	$\pi_{-6} \rightarrow \pi_1^*$	4.81	inactive	4.10	inactive	4.81	inactive		
^1B_u	$\pi_{-1} \rightarrow \pi_5^*$	4.94	0.4512	4.22	0.0361	4.83	0.6432	4.68 (265.1)[c] 4.60 (269.5)[d]	0.029[c]
^1A_g	$\pi_{-1} \rightarrow \pi_6^*$	4.94	inactive	4.25	inactive	4.90	inactive		
^1B_u	$\pi_{-2} \rightarrow \pi_2^*$	5.00	0.6111	4.53	1.0414	4.88	0.0337	4.95 (250.6)[c]	0.019[c]
^1A_g	$\pi_{-3} \rightarrow \pi_4^*$	5.21	inactive	4.62	inactive	5.20	inactive		
^1B_u	$\pi_{-3} \rightarrow \pi_3^*$	5.31	0.4491	4.69	0.0113	5.21	0.3694		
^1A_g	$\pi_{-7} \rightarrow \pi_1^*$	5.43	inactive	4.75	inactive	5.41	inactive		
^1B_u	$\pi_{-3} \rightarrow \pi_4^*$	5.45	0.3118	4.77	0.0607	5.41	0.0715		
^1B_u	$\pi_{-5} \rightarrow \pi_2^*$	5.61	0.0086	5.00	0.0111	5.61	0.0039		
^1A_g	$\pi_{-4} \rightarrow \pi_2^*$	5.67	inactive	5.00	inactive	5.50	inactive		
^1A_g	$\pi_{-6} \rightarrow \pi_2^*$	5.91	inactive	–	–	–	–		

[a] All calculations were performed using the 6-31G(d,p) standard basis set. The ground-state wave function transforms as the ^1A_g irreducible representation of the C_{2h} point group. [b] The orbitals are numbered in the order of increasing orbital energies with π_{-1} and π_1^* being the highest occupied and lowest unoccupied orbitals, respectively. [c] This work, wavelengths in nanometers are given in parentheses. [d] Reference 14, wavelengths in nanometers are given in parentheses, and the spectrum was recorded from the solid mixture of *n*-hexane and DBC at 77 K.

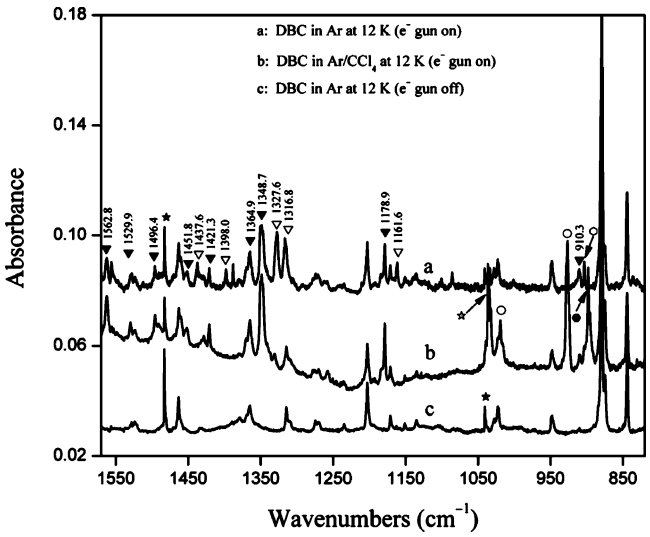

Figure 4. Observed IR absorption spectra of neutral and ionic DBC (Ar, 12 K). Bands marked with ▼ are assigned to DBC cations, and DBC anions are labeled with ▽. (a) IR spectrum of DBC neutrals, cations, and anions. (b) IR spectrum of DBC neutrals and cations. (c) IR spectrum of DBC neutrals. Bands marked with ★ (1483.2, 1040.7 cm^{-1}) are due to impurities. Bands marked by ☆, ○, ♦, and ♢ are attributed to CCl_3^+ (1036.5 cm^{-1}),[24] CCl_3·Cl (1019.3 cm^{-1}, 926.5 cm^{-1}),[25] CCl_3 (898.0 cm^{-1}),[26] and HAr_2^+ (903.3 cm^{-1}) radicals, respectively.[27]

and half Lorentzian character and a 3 cm^{-1} bandwidth, was situated at every frequency observed for a DBC ion. Theoretical spectra were generated in the same way, with a scaling factor of 0.978. As shown in Figure 5, the observed frequencies are in good overall agreement with predictions. The predicted strong anionic absorption at ~1558 cm^{-1} is absent in the experimental spectrum, perhaps because of the overlap with the strong water absorption in this range. In addition, some of the DBC anion bands are photosensitive, making DBC^- band assignments in this region difficult.

TABLE 3: Comparison of the Calculated (B3LYP/6-31G(d,p)) and Experimental (Ar Matrix, 12 K) Infrared Absorption Bands (in cm^{-1}) of Dibenzo[*b*,*def*]chrysene Radical Cation in the ^2B_g Electronic Ground State

symmetry	mode description[a]	ν_{cal}[b,c]	ν_{exp}[b]
a_u	ϵ(C−C−H) + τ(C−C−C)	467.2 (0.02)	
b_u	α(C−C−C)	561.2 (0.03)	
a_u	ϵ(C−C−H)	757.1 (0.20)	
a_u	ϵ(C−C−H)	821.5 (0.02)	
a_u	ϵ(C−C−H)	863.3 (0.02)	
a_u	ϵ(C−C−H)	902.9 (0.07)	910.3 (0.13)
b_u	β(C−C−H)	1186.0 (0.34)	1178.9 (0.69)
b_u	β(C−C−H)	1207.9 (0.05)	
b_u	β(C−C−H) + R(C−C)	1260.3 (0.03)	
b_u	R(C−C) + β(C−C−H)	1304.6 (0.04)	
b_u	R(C−C)	1352.9 (1.00)	1348.7 (1.00)
b_u	R(C−C)	1371.6 (0.14)	1364.9 (0.19)
b_u	β(C−C−H)	1428.1 (0.12)	1421.3 (0.28)
b_u	β(C−C−H) + R(C−C)	1434.4 (0.02)	
b_u	R(C−C) + β(C−C−H)	1463.6 (0.04)	1451.8 (0.08)
b_u	R(C−C) + β(C−C−H)	1498.3 (0.34)	1496.4 (0.25)
b_u	R(C−C) + β(C−C−H)	1539.1 (0.11)	1529.9 (0.11)
b_u	R(C−C)	1563.0 (0.17)	
b_u	R(C−C)	1565.9 (0.54)	1562.8 (0.47)
b_u	R(C−C)	1607.5 (0.20)	
b_u	r(C−H)	3151.8 (0.02)	
b_u	r(C−H)	3157.4 (0.02)	
b_u	r(C−H)	3171.4 (0.02)	

[a] Notation used: R and r are stretching modes, α and β are in-plane bending modes, and τ and ϵ are out-of-plane vibrations. [b] Relative IR intensities for predicted and experimental frequencies are given in parentheses. [c] Frequencies scaled by a factor of 0.978. The bands with relative intensities equal to 0.02 or higher are listed only. The integral intensity predicated for the 1352.9 cm^{-1} band is equal to 500 km/mol.

TABLE 4: Comparison of the Calculated (B3LYP/6-31G(d,p)) and Experimental (Ar Matrix, 12 K) Infrared Absorption Bands (in cm^{-1}) of Dibenzo[*b,def*]chrysene Radical Anion in the ^2A_u Electronic Ground State

symmetry	mode description[a]	ν_{cal}[b,c]	ν_{exp}[b]
b_u	α(C−C−C)	466.5 (0.06)	
a_u	ϵ(C−C−H)	709.8 (0.05)	
b_u	α(C−C−C)	746.7 (0.04)	
a_u	ϵ(C−C−H)	752.6 (0.08)	
a_u	ϵ(C−C−H)	794.6 (0.07)	
a_u	ϵ(C−C−H)	824.2 (0.02)	
b_u	R(C−C) + β(C−C−H)	986.1 (0.03)	
b_u	R(C−C) + β(C−C−H)	1033.9 (0.05)	
b_u	β(C−C−H)	1152.0 (0.03)	
b_u	β(C−C−H)	1174.6 (0.22)	1161.6 (0.35)
b_u	β(C−C−H)	1187.8 (0.02)	
b_u	β(C−C−H) + R(C−C)	1245.5 (0.02)	
b_u	R(C−C) + β(C−C−H)	1289.2 (0.06)	
b_u	R(C−C)	1323.1 (0.29)	1316.8 (0.32)
b_u	R(C−C)	1336.2 (1.00)	1327.8 (1.00)
b_u	R(C−C) + β(C−C−H)	1407.0 (0.12)	1398.0 (0.23)
b_u	R(C−C) + β(C−C−H)	1416.2 (0.02)	
b_u	R(C−C) + β(C−C−H)	1450.7 (0.24)	1437.6 (0.42)
b_u	R(C−C) + β(C−C−H)	1488.4 (0.04)	
b_u	R(C−C) + β(C−C−H)	1527.5 (0.04)	
b_u	R(C−C)	1558.0 (0.54)	
b_u	R(C−C)	1563.8 (0.03)	
b_u	R(C−C)	1592.9 (0.08)	
b_u	r(C−H)	3073.7 (0.02)	
b_u	r(C−H)	3082.5 (0.10)	
b_u	r(C−H)	3090.0 (0.19)	
b_u	r(C−H)	3102.7 (0.31)	
b_u	r(C−H)	3114.6 (0.06)	
b_u	r(C−H)	3128.0 (0.25)	

[a] Notation used: R and r are stretching modes, α and β are in-plane bending modes, and τ and ϵ are out-of-plane vibrations. [b] Relative IR intensities for predicted and experimental frequencies are given in parentheses. [c] Frequencies scaled by a factor of 0.978. The bands with relative intensities equal to 0.02 or higher are listed only. The integral intensity predicated for the 1336.2 cm^{-1} band is equal to 679 km/mol.

It is well-known that photolysis results in a decrease in ion absorption in matrixes. The effects of photolysis on the DBC ions are shown in Figure 6. Before photolysis, the average $[DBC^+]/[DBC^-]$ ratio is about 1.2. After 1 min of photolysis, the intensity ratio rises to ~2. On further photolysis (5 min), the ratio increases to 4. After still longer UV exposure (45 min), the DBC anions have disappeared whereas the DBC cations remain at ~30% of their original intensity. Overall, DBC anions are more sensitive than cations to UV light. Electrons photodetached from DBC^- are partially scavenged by cations in the matrix (DBC^+ and impurities such as HAr_2^+) and by species with nonzero electron affinities (DBC and neutral impurities such as OH (EA = 1.8 eV)).[33] Only a portion of the electrons photodetached from DBC^- are recaptured by DBC^+ radicals because of various competitive electron capture processes. Overall, the photodissociation yield of DBC^- is larger than for DBC^+.

2. Electronic Absorption Spectra. Electronic and vibrational spectra were recorded on the same sample/matrixes. Figure 7 shows the optical spectra, and Figure 4 shows the corresponding infrared spectra. Calculated and observed electronic transition energies for DBC cations and anions are compared in Tables 5 and 6, respectively. The effect of UV photolysis on DBC ion concentrations is displayed in Figure 8.

Electron bombardment of a DBC/CCl_4/Ar mixture produced several new electronic transitions (compare Figure 7, b and c) at 805.0 nm (1.54 eV), 648.3 nm (1.91 eV), 626.3 nm (1.98 eV), and 589.3 nm (2.10 eV), all of which are here assigned to

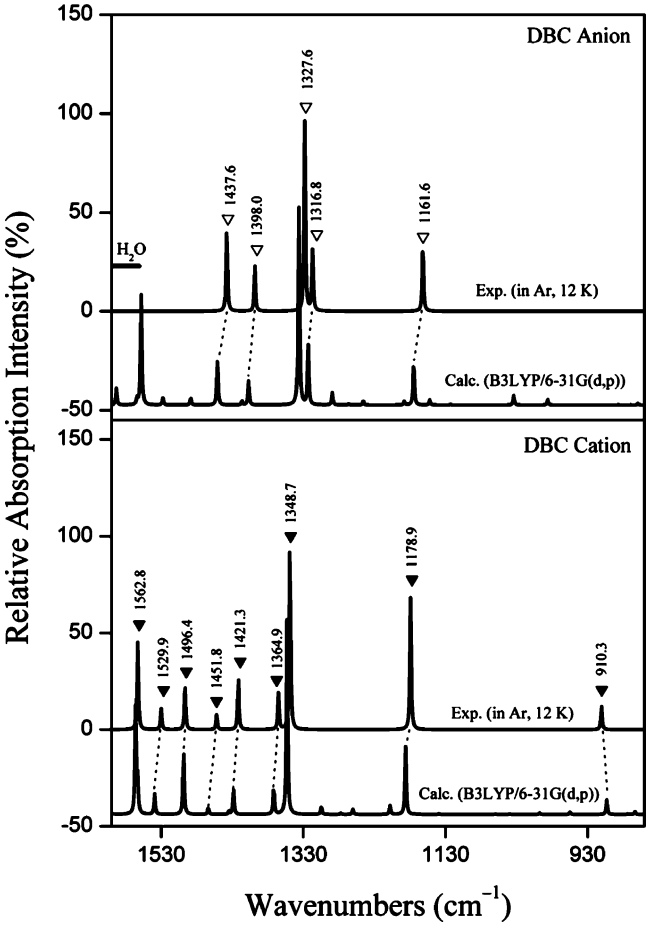

Figure 5. Synthetic experimental and calculated IR absorption spectra for DBC cations and anions. Experimental IR spectra for ions were synthesized from frequencies and relative intensities observed in the Ar matrix at 12 K of Figure 4. The predicted IR spectra were computed at B3LYP/6-31G(d,p) level and scaled by 0.978. Strong water absorption region is marked by the horizontal solid line.

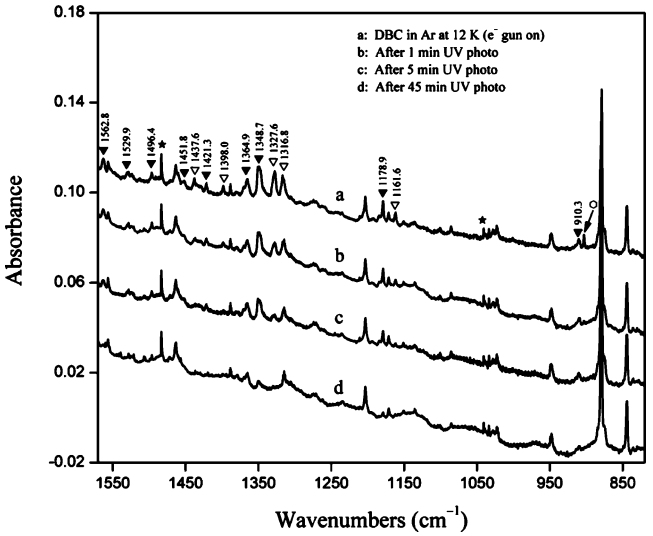

Figure 6. Experimental IR spectra for DBC species (Ar, 12 K) under different photolysis time. The DBC^+ and DBC^- bands are marked by ▼ and ▽, respectively. Notation for other bands is the same as in Figure 4.

DBC cation transitions. The first band (1.54 eV), assigned to the $D_2(^2A_u) \leftarrow D_0(^2B_g)$ transition, is within 0.06 eV of the theoretical prediction (cf. Table 5). The strong progression starting at 648.3 nm (and including bands at 626.3 and 589.3

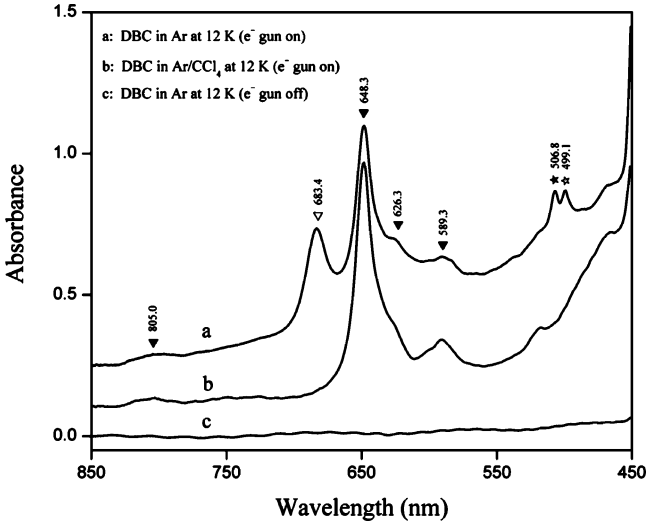

Figure 7. Observed optical absorption spectra of neutral and ionic DBC in Ar at 12 K. Bands marked with ▼ are assigned to DBC cations, and DBC anions are labeled with ▽. (a) Optical spectrum of DBC neutrals, cations, and anions. (b) Optical spectrum of DBC neutrals and cations. (c) Optical spectrum of DBC neutrals. Carriers of the bands marked by ☆ are unknown.

nm) is assigned to $D_3(^2A_u) \leftarrow D_0(^2B_g)$. A similar strong absorption was reported by Shida[10,34] for DBC^+ at 653 nm in *sec*-butyl chloride. Predicted ground-state fundamental Raman frequencies of 544 cm^{-1} (231 $Å^4$/amu) and 1564 cm^{-1} (1284 $Å^4$/amu), calculated at the B3LYP/6-31G(d,p) level, are close to the observed D_3 state intervals of 542 and 1544 cm^{-1}.

A comparison of Figure 7, a and b shows three new bands at 683.4 nm (1.81 eV), 506.8 nm (2.45 eV), and 499.1 nm (2.48 eV). The 683.4 nm band is assigned to the $D_4(^2B_g) \leftarrow D_0(^2A_u)$ transition of the DBC anion, and the origin of two other bands is unknown. The latter two bands (506.8 and 499.1 nm) show up only when DBC anions are created. They are not sensitive to UV photolysis. Figure 8 shows that only after longtime UV matrix irradiation do the ratio of these two peaks vary slightly. As shown in Figure 8, the intensities of the DBC ionic electronic absorption vary with the same pattern as the infrared intensities in Figure 6. As mentioned above, prolonged (i.e., 45 min) photolysis results in a DBC cation signal decrease of 70% and a complete disappearance of the DBC anion signal. This observation supports the vibrational band assignments to the two ions made from the analysis of the infrared spectra, and vice versa.

Shida previously observed a band at 442 nm (2.81 eV) in solid 2-methyltetrahydrofuran (at 77 K) and assigned it to the DBC anion. The intensity of this band was even greater than the transition at 690 nm.[10,34] However, in our experiments, this band is overlapped by the strong absorption of neutral DBC. Although there is a predicted electronic transition $[D_8(^2B_g) \leftarrow D_0(^2A_u)]$ at ~2.8 eV, its oscillator strength is much smaller than for the $D_4 \leftarrow D_0$ transition. Thus, there is not enough information from our experiment to confirm this assignment.

C. Astrochemistry Implications. The formation yields of PAH ions are dependent on their ionization energies (IE) and electron affinities (EA). Experimentally, the IE of DBC lies between 6.8 and 7.4 eV.[35,36] We have calculated an adiabatic IE of 6.19 eV and a vertical IE of 6.24 eV (B3LYP/6-31G(d,p) level). This IE is typical of many PAHs and indicates the high probability of DBC ionization upon exposure to UV−visible or cosmic ray radiation.

The calculated adiabatic EA for DBC is 0.89 eV, and the vertical EA is 0.79 eV (B3LYP/6-31G(d,p)). An experimental EA of 1.1 eV has been reported.[31] The DFT approach usually gives computed electron affinities within 0.3 eV of the experimental value.[37] Diffuse functions are not really important in improving estimated electron affinities for large PAH systems.[38] With such a high electron affinity, DBC anions should easily form in the electron-rich conditions of interstellar space, such as the envelope of stars.

1. The Unidentified Infrared (UIR) Emission Bands. Infrared absorption band energies and intensity distributions for DBC cations and anions are quite different from neutral DBC. Many of the infrared absorption bands observed for the DBC ions are in line with the unidentified interstellar infrared (UIR) emission features. Figure 9 shows that a mixture of DBC species (26% neutral, 7% anion, and 67% cation) resembles reasonably well the UIR bands observed from the reflection nebula NGC 7023,[39,40] although the relative intensities of the bands in the 600−1000 cm^{-1} region are inverted compared to those of the UIR bands. The strongest absorption bands at 1348.7 cm^{-1} (7.4 μm) and 1327.8 cm^{-1} (7.5 μm) for the DBC cation and anion, respectively, correlate reasonably well with the most intense UIR broad band at 7.7 μm. The 910.3 cm^{-1} (11.0 μm) DBC

TABLE 5: Calculated and Observed Vertical Excitation Energies, ω, and Oscillator Strengths, f, for Dibenzo[*b*,*def*]chrysene Cation[a]

		NWCHEM				Gaussian 98			
		B3LYP(AC)		BLYP		B3LYP		experiment	
state	transition[b]	ω/eV	f	ω/eV	f	ω/eV	f	ω/eV	f
^2B_g	$\pi_{-2} \rightarrow \pi_0^*$	1.45	inactive	1.26	inactive	1.43	inactive		
^2A_u	$\pi_{-1} \rightarrow \pi_0^*$	1.55	0.0728	1.42	0.0613	1.48	0.0524	1.54 (805.0)[c] 1.38 (900)[d]	0.002[c]
^2A_u	$\pi_{-3} \rightarrow \pi_0^*$	2.18	0.2128	2.00	0.0312	2.04	0.2448	1.91 (648.3)[c] 1.90 (653)[d]	0.11[c]
^2A_u	$\pi_{-3} \rightarrow \pi_0^*$	2.29	0.1103	2.07	0.1750	2.26	0.0233		
^2B_g	$\pi_{-4} \rightarrow \pi_0^*$	2.52	inactive	2.23	inactive	2.46	inactive		
^2A_u	$\pi_{-5} \rightarrow \pi_0^*$	2.60	0.1469	2.33	0.1555	2.51	0.0577		
^2B_g	$\pi_{-2} \rightarrow \pi_1^*$	2.91	inactive	2.65	inactive	2.80	inactive		
^2A_u	$\pi_{-1} \rightarrow \pi_1^*$	3.00	0.0507	2.68	0.0174	2.94	0.0606		
$^{-2}A_u$	$\pi_0 \rightarrow \pi_2^*$	3.33	0.0166	2.97	0.0122	3.25	0.0156		
^2A_u	$\pi_{-6} \rightarrow \pi_0^*$	3.39	0.0213	3.07	0.0284	3.37	0.0029		

[a] All calculations were performed using the 6-31G(d,p) standard basis set. The ground-state wave function transforms as the ^2B_g irreducible representation of C_{2h} point group. [b] The orbitals are numbered in the order of increasing orbital energies with π_{-1}, π_0, π_0^*, and π_1^* being the highest doubly occupied, highest occupied, highest unoccupied, and lowest doubly unoccupied orbitals, respectively. [c] This work, wavelengths in nanometers are given in parentheses. [d] References 10, 34, wavelengths in nanometers are given in parentheses.

TABLE 6: Calculated and Observed Vertical Excitation Energies, ω, and Oscillator Strengths, f, for Dibenzo[*b,def*]chrysene Anion[a]

		NWCHEM				Gaussian 98			
		B3LYP(AC)		BLYP		B3LYP		experiment	
state	transition[b]	ω/eV	f	ω/eV	f	ω/eV	f	ω/eV	f
^2A_u	$\pi_0 \rightarrow \pi_2^*$	1.42	inactive	1.22	inactive	1.37	inactive		
^2B_g	$\pi_0 \rightarrow \pi_1^*$	1.52	0.0713	1.37	0.0624	1.44	0.0518		
^2B_g	$\pi_0 \rightarrow \pi_3^*$	2.16	0.0764	1.94	0.0173	2.12	0.0342		
^2B_g	$\pi_{-1} \rightarrow \pi_0^*$	2.20	0.2777	2.06	0.2457	2.00	0.2352	1.81 (683.4)[c] 1.80 (690)[d]	0.11[c]
^2A_u	$\pi_0 \rightarrow \pi_4^*$	2.58	inactive	2.29	inactive	2.53	inactive		
^2B_g	$\pi_0 \rightarrow \pi_5^*$	2.66	0.0864	2.38	0.0714	2.60	0.0374		
^2A_u	$\pi_{-1} \rightarrow \pi_3^*$	2.88	inactive	2.60	inactive	2.80	inactive		
^2B_g	$\pi_{-1} \rightarrow \pi_1^*$	2.94	0.0597	2.62	0.0160	2.89	0.0569	2.81 (442)[d]	
^2B_g	$\pi_{-2} \rightarrow \pi_0^*$	3.32	0.0107	2.92	0.0290	3.29	0.0095		
^2A_u	$\pi_{-3} \rightarrow \pi_0^*$	3.34	inactive	2.86	inactive	3.30	inactive		

[a] NWCHEM calculations were performed using the 6-31++G(d,p) standard basis set, whereas the 6-31G(d,p) basis set was used in Gaussian 98 calculations. The ground-state wave function transforms as the ^2A_u irreducible representation of the C_{2h} point group. [b] The orbitals are numbered in the order of increasing orbital energies with π_{-1}, π_0, π_0^*, and π_1^* being the highest doubly occupied, highest occupied, highest unoccupied, and lowest doubly unoccupied orbitals, respectively. [c] This work, wavelengths in nanometers are given in parentheses. [d] References 10, 34, wavelengths in nanometers are given in parentheses.

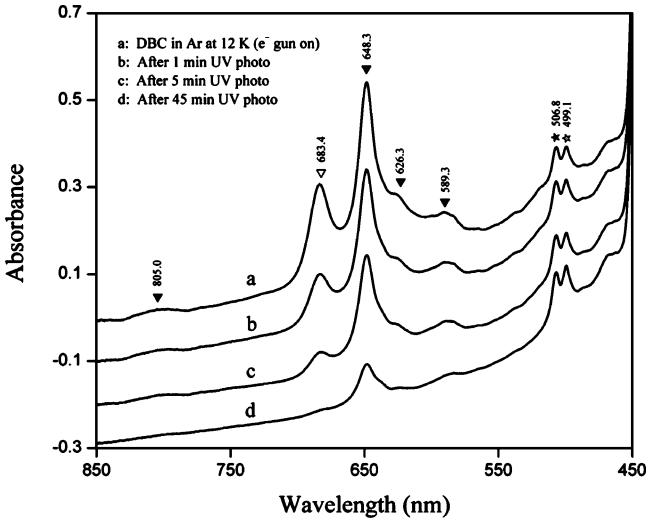

Figure 8. Experimental optical spectra (corresponding to Figure 6 IR spectra) for DBC species trapped in Ar at 12 K under different photolysis times.

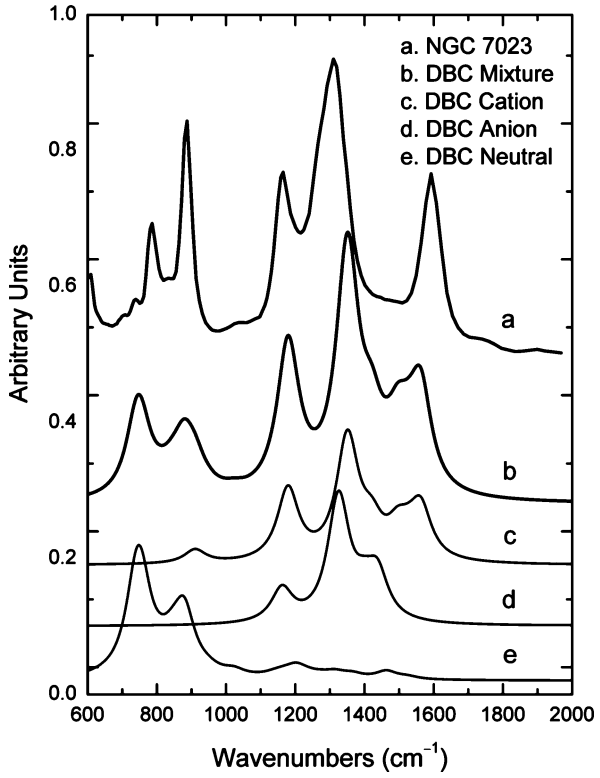

Figure 9. Comparison of UIR bands from the reflection nebula NGC 7023 with a mixture of DBC species (26% neutral, 7% anion, and 67% cation). (a) UIR bands from NGC 7023 (adapted, with permission, from refs 39 and 40); (b) Mixture of DBC species (i.e., sum of spectra c−e); (c) DBC cation IR spectrum; (d) DBC anion IR spectrum; (e) neutral DBC IR spectrum. Spectra c−e were constructed from the experimental spectrum of each species (neutral, cation, or anion) in the 600−2000 cm^{-1} range by increasing every peak bandwidth (fwhm) to 75 cm^{-1}. Latter value was chosen because it is the experimental bandwidth of the most intense UIR band at 7.7 μm (1298 cm^{-1}).

cation band is close to the 11.0 μm emission feature. The 1178.9 cm^{-1} (8.5 μm) peak may contribute to the 8.6 μm UIR band, whereas the 1562.8 cm^{-1} (6.4 μm) band may contribute to the 6.2 μm UIR peak.

The DBC anion absorption at 1161.6 cm^{-1} (8.6 μm) may account for the 8.6 μm emission feature. The 1316 cm^{-1} (7.6 μm), 1398.0 cm^{-1} (7.2 μm), and 1437.6 cm^{-1} (7.0 μm) bands fit within the broad UIR envelope between 6.2 μm and 7.6 μm. The predicted band at 1558.0 cm^{-1} (6.4 μm) may correspond to the 6.2 μm UIR feature.

The 3 μm region of the UIR bands is not discussed here for two reasons. First, three broad absorption bands have been recorded for DBC in the C−H stretch region but their assignments are considered very tentative, and second, spectra recorded for NGC 7023 do not include this region.[39,40]

Although the DBC IR bands fall in close proximity to the UIR bands, our values are, of course, from Ar matrixes and thus subject to some shifts compared to gas-phase values. What are the magnitudes of the expected shifts? Recently, IR spectra in the C−H stretching region were reported[41] for a few small PAHs seeded into supersonically expanded carrier gases with low rotational (10 K) and vibrational (<50 K) temperatures. These results show that red-shifts averaging 0.5−4.4 cm^{-1}, going from the gas phase to the Ar matrixes, can be expected. Based on Jacox's compilation[42] of gas-to-Ar matrix shifts for numerous neutral and ionic species, dramatic changes in the absorption energies of PAH ions in the mid-IR region are not expected with a change of phase. Thus, the Ar matrix-to-gas shifts are expected to be too small to affect the two significant digits quoted in the UIR band positions listed above.

In summary, a mixture of DBC neutrals, cations, and anions does a passable job of mimicking the UIR features of NGC 7023, which lends credence to our conclusion that such a mixture may contribute to the UIR emission features of this and other UIR sources.

2. The Diffuse Interstellar Bands (DIBs). PAHs and their ions have also been proposed as possible carriers of the visible diffuse interstellar absorption bands (DIBs).[43] A number of large PAHs, such as dicoronylene ($C_{48}H_{20}$), have been studied and compared with the DIB spectra.[43] Although neutral DBC possesses no electronic transitions that match the DIB bands, its ions do. The most intense DCB cation electronic band at 648.3 nm (Ar/12 K) and anion band at 683.4 nm (Ar/12 K) are in close proximity to the DIB bands at 649.4 and 683.4 nm, respectively, observed from HD 183143.[44] Matrix-to-gas shifts must be considered. The electronic absorption bands of PAH cations usually red-shift in matrixes compared to the absorption in the gas phase. For example, the shift is 120 cm^{-1} for naphthalene,[45] 218 cm^{-1} for acenaphthene,[45] 393 cm^{-1} for pyrene,[45,46] 289 cm^{-1} for fluorene,[47] and 266 cm^{-1} for anthracene.[48] Adopting an average gas-to-Ar matrix shift of 250 cm^{-1}, the electronic bands for DBC cations and anions should appear in the gas phase at 638.0 and 676.5 nm, respectively. Compared to the DIB bands measured in the interstellar source HD 183143,[44] DBC cations may thus contribute to the diffuse bands at 636.7, 637.6, and 637.9 nm, and DBC anions could be the carrier of the DIB bands at 676.8, 676.9, 677.0, and 677.9 nm. Therefore, the DBC ions should be viewed as potential contributors to the DIB bands as well as to the UIR bands.

V. Conclusions

(1) The vibrational and electronic spectra of neutral DBC were recorded in argon matrixes at 12 K. Band assignments were made by comparison with theoretical calculations. Out-of-plane C−C−H bending vibrations at 740.6 and 878.8 cm^{-1} were among the strongest modes observed. Five electronic transitions have been observed for neutral DBC, with the first [assigned to the $S_1(^1B_u) \leftarrow S_0(^1A_g)$ transition] lying at 438.8 nm and the strongest [assigned to the $S_7(^1B_u) \leftarrow S_0(^1A_g)$ transition] located at 305.5 nm. The vibrational structures for these two bands were also observed and assigned.

(2) Infrared and optical spectra of the DBC cation and anion are reported for the first time. The electronic and vibrational spectra were recorded on the same matrix, allowing an estimate of the oscillator strengths of the observed electronic transitions. The IR band assignments were supported not only by theoretical predictions but also by intensity correlation with visible band intensities. The strongest IR bands of the DBC cations and anions lie at 1348.7 and 1327.8 cm^{-1}, respectively. The electronic band at 648.3 nm has been assigned to the DBC cation $D_3(^2A_u) \leftarrow D_0(^2B_g)$ transition, and the band at 683.4 nm has been assigned to the DBC anion $D_4(^2B_g) \leftarrow D_0(^2A_u)$ transition. The photodissociation rate for DBC anions is higher than for cations.

(3) Comparison of the observed infrared and visible bands of the DBC cations and anions with the interstellar UIR and DIB bands reveals that DBC ions may be contributors to both sets of bands.

Acknowledgment. We gratefully acknowledge the National Aeronautics and Space Administration for its support of this research and thank Professor K. Sellgren for her assistance with the adaptation of the spectrum of NGC 7023, shown in Figure 9. This work was also supported by the U.S. Department of Energy under Grant No. DE-FG02-04ER15621.

References and Notes

(1) Dipple, A. ACS Symposium Series 283; American Chemical Society: Washington, DC, 1985; p 1.
(2) Bostrom, C. E.; Gerde, P.; Hanberg, A.; Jernstrom, B.; Johansson, C.; Kyrklund, T.; Rannug, A.; Tornqvist, M.; Victorin, K.; Westerholm, R. *Environ. Health Perspect.* **2002**, *110*, 451.
(3) Lopes, W. A.; deAndrade, J. B. *Quim. Nova* **1996**, *19*, 497.
(4) Zimmermann, R.; Heger, H. J.; Kettrup, A.; Nikolai, U. *Fresenius' J. Anal. Chem.* **2000**, *366*, 368
(5) Leger, A.; Puget, J. L. *Astron. Astrophys.* **1984**, *137*, L5.
(6) Allamandola, L. J.; Tielens, A. G. G. M.; Barker, J. R. *Astrophys. J.* **1985**, *290*, L25.
(7) d'Hendecourt, L.; Ehrenfreund, P. *Life Sci.: Complex Org. Space* **1997**, *19*, 1023.
(8) Rapacioli, M.; Joblin, C.; Boissel, P. *Astron. Astrophys.* **2005**, *429*, 193 and references therein.
(9) Allamandola, L. J.; Tielens, A. G. G. M.; Barker, J. R. *Astrophys. J., Suppl. Ser.* **1989**, *71*, 733.
(10) Shida, T.; Iwata, S. *J. Am. Chem. Soc.* **1973**, *95*, 3473.
(11) Barone, P. M. V. B.; Camilo, A., Jr.; Galvao, D. S. *Phys. Rev. Lett.* **1996**, *77*, 1186.
(12) Andersen, K. B.; Waluk, J.; Thulstrup, E. W. *Photochem. Photobiol.* **1999**, *69*, 158.
(13) Dibenzo[*b*,*def*]chrysene. http://chrom.tutms.tut.ac.jp/JINNO/DATABASE/07dibenzo[*b*,*def*]chrysene.html
(14) Nakimovsky, L. A.; Lamotte, M.; Joussot-Dubien, J. *Handbook of Low-Temperature Electronic Spectra of Polycyclic Aromatic Hydrocarbons;* Elsevier: New York, 1989.
(15) Szczepanski, J.; Banisaukas J.; Vala, M.; Hirata, S.; Bartlett, R. J.; Head-Gordon, M. *J. Phys. Chem. A* **2002**, *106*, 63.
(16) Frisch, M. J.; Trucks, G. W.; Schlegel, H. B.; Scuseria, G. E.; Robb, M. A.; Cheeseman, J. R.; Zakrzewski, V. G.; Montgomery, J. A., Jr.; Stratmann, R. E.; Burant, J. C.; Dapprich, S.; Millam, J. M.; Daniels, A. D.; Kudin, K. N.; Strain, M. C.; Farkas, O.; Tomasi, J.; Barone, V.; Cossi, M.; Cammi, R.; Mennucci, B.; Pomelli, C.; Adamo, C.; Clifford, S.; Ochterski, J.; Petersson, G. A.; Ayala, P. Y.; Cui, Q.; Morokuma, K.; Malick, D. K.; Rabuck, A. D.; Raghavachari, K.; Foresman, J. B.; Cioslowski, J.; Ortiz, J. V.; Baboul, A. G.; Stefanov, B. B.; Liu, G.; Liashenko, A.; Piskorz, P.; Komaromi, I.; Gomperts, R.; Martin, R. L.; Fox, D. J.; Keith, T.; Al-Laham, M. A.; Peng, C. Y.; Nanayakkara, A.; Gonzalez, C.; Challacombe, M.; Gill, P. M. W.; Johnson, B.; Chen, W.; Wong, M. W.; Andres, J. L.; Gonzalez, C.; Head-Gordon, M.; Replogle, E. S.; Pople, J. A. *Gaussian 98*; Gaussian Inc., Pittsburgh, PA, 1998.
(17) Straatsma, T. P.; Aprà, E.; Windus, T. L.; Dupuis, M.; Bylaska, E. J.; de Jong, W.; Hirata, S.; Smith, D. M. A. M.; Hackler, T.; Pollack, L.; Harrison, R. J.; Nieplocha, J.; Tipparaju, V.; Krishnan, M.; Auer, A. A.; Brown, E.; Cisneros, G.; Fann, G. I.; Fruchtl, H.; Garza, J.; Hirao, K.; Kendall, R.; Nichols, J. A.; Tsemekhman, K.; Valiev, M.; Wolinski, K.; Anchell, J.; Bernholdt, D.; Borowski, P.; Clark, T.; Clerc, D.; Dachsel, H.; Deegan, M.; Dyall, K.; Elwood, D.; Glendening, E.; Gutowski, M.; Hess, A.; Jaffe, J.; Johnson, B.; Ju, J.; Kobayashi, R.; Kutteh, R.; Lin, Z.; Littlefield, R.; Long, X.; Meng, B.; Nakajima, T.; Niu, S.; Rosing, M.; Sandrone, G.; Stave, M.; Taylor, H.; Thomas, G.; Lenthe, van J.; Wong, A.; Zhang, Z. *NWCHEM, A Computational Chemistry Package for Parallel Computers*; Pacific Northwest National Laboratory: Richland, WA, 2003.
(18) Hirata, S.; Head-Gordon, M.; Szczepanski, J.; Vala, M. *J. Phys. Chem. A* **2003**, *107*, 4940 and references therein.
(19) Hirata, S.; Zhan, C. G.; Aprà, E.; Windus, T.; Dixon, D. A. *J. Phys. Chem. A* **2003**, *107*, 10154.
(20) Zhan, C. G.; Nichols, J. A.; Dixon, D. A.; *J. Phys. Chem. A* **2003**, *107*, 4184.
(21) Banisaukas, J.; Szczepanski, J.; Vala, M.; Hirata, S. *J. Phys. Chem. A* **2004**, *108*, 3713.
(22) Szczepanski, J.; Dibben, M. J.; Pearson, W.; Eyler, J. R.; Vala, M. *J. Phys. Chem. A* **2001**, *105*, 9388.
(23) Parac, M.; Grimme, S. *Chem. Phys.* **2003**, *292*, 11.
(24) Jacox, M. E.; Milligan, D. E. *J. Chem. Phys.* **1971**, *54*, 3935
(25) Andrews, L.; Prochaska, F. T. *J. Phys. Chem.* **1979**, *83*, 368.
(26) Andrews, L. *J. Phys. Chem.* **1967**, *71*, 2761.
(27) Bondybey, V. E.; Pimentel, G. C. *J. Chem. Phys.* **1972**, *56*, 3832.
(28) Lacmann, K.; Maneira, M. J. P.; Moutinho, A. M. C.; Weigman, U. *J. Chem. Phys.* **1983**, *78*, 1767.
(29) Scheunemann, H. U.; Illenberger, E.; Baumgartel, H. *Ber. Bunsen-Ges.* **1980**, *84*, 580.
(30) Martin, J. D. D.; Hepburn, J. W. *J. Chem. Phys.* **1998**, *109*, 8139.
(31) Briegleb, G. *Angew. Chem.* **1964**, *76*, 326.
(32) Szczepanski, J.; Wehlburg, C.; Vala, M. *Chem. Phys. Lett.* **1995**, *232*, 221.

(33) Schulz, P. A.; Mead, R. D.; Jones, P. L.; Lineberger, W. C. *J. Chem. Phys.* **1982**, *77*, 1153.

(34) Shida, T. *Electronic Absorption Spectra of Radical Ions*; Elsevier: Amsterdam, 1988.

(35) Clar, E.; Schmidt, W. *Tetrahedron* **1979**, *35*, 1027.

(36) Clar, E.; Schmidt, W. *Tetrahedron* **1976**, *32*, 2563.

(37) Xie, Y.; Schaefer, H. F., III; Wang, Y.; Fu, X.; Liu, R. *Mol. Phys.* **2000**, *98*, 279 and references therein.

(38) Gonzales, J. M.; Barden, C. J.; Brown, S. T.; Schleyer, P. von R.; Schaefer, H. F., III; Li, Q. S. *J. Am. Chem. Soc.* **2003**, *125*, 1064.

(39) Cesarsky, D.; Lequeux, J.; Abergel, A.; Perault, M.; Palazzi, E.; Madden, S.; Tran, D. *Astron. Astrophys.* **1996**, *315*, L305.

(40) Sellgren, K. *Spectrochim. Acta* **2001,** *57*, 627.

(41) Huneycutt, A. J.; Casaes, R. N.; McCall, B. J.; Chung, C. Y.; Lee, Y. P.; Saykally, R. *ChemPhysChem* **2004**, *5*, 321.

(42) Jacox, M. E. *Chem. Soc. Rev.* **2002**, *31*, 108.

(43) Ruiterkamp, R.; Halasinski, T.; Salama, F.; Foing, B. H.; Allamandola, L. J.; Schmidt, W.; Ehrenfreund, P. *Astron. Astrophys.* **2002**, *390*, 1153 and references therein.

(44) Herbig, G. H. *Annu. Rev. Astrophys.* **1995**, *33*, 19.

(45) Biennier, L.; Salama, F.; Allamandola, L. J.; Scherer, J. J. *J. Chem. Phys.* **2003**, *118*, 7863.

(46) Biennier, L.; Salama, F.; Gupta, M.; O'Keefe, A. *Chem. Phys. Lett.* **2004**, *387*, 287.

(47) Pino, T.; Brechignac, P.; Dartois, E.; Demyk, K.; d'Hendecourt, L. *Chem. Phys. Lett.* **2001**, *339*, 64.

(48) Sukhorukov, O.; Staicu, A.; Diegel, E.; Rouille, G.; Henning, Th.; Huisken, F. *Chem. Phys. Lett.* **2004**, *386*, 259.